Annals of Biomedical Engineering, Vol. 44, No. 12, December 2016 *(© 2016)* pp. 3522–3538
DOI: 10.1007/s10439-016-1695-2

Three-Dimensional Tricuspid Annular Motion Analysis from Cardiac Magnetic Resonance Feature-Tracking

SHUANG LENG,[1] MENG JIANG,[2] XIAO-DAN ZHAO,[1] JOHN CARSON ALLEN,[3] GHASSAN S. KASSAB,[4] RONG-ZHEN OUYANG,[5] JU-LE TAN,[1] BEN HE,[2] RU-SAN TAN,[1,3] and LIANG ZHONG[1,3]

[1]National Heart Centre Singapore, 5 Hospital Drive, Singapore 169609, Singapore; [2]Department of Cardiology, Renji Hospital, School of Medicine, Shanghai Jiaotong University, Shanghai 200001, People's Republic of China; [3]Duke-NUS Medical School, 8 College Road, Singapore 169857, Singapore; [4]California Medical Innovations Institute, San Diego, CA 92121, USA; and [5]Department of Radiology, Renji Hospital, School of Medicine, Shanghai Jiaotong University, Shanghai 200001, People's Republic of China

(Received 2 March 2016; accepted 7 July 2016; published online 19 July 2016)

Associate Editor Estefanía Peña oversaw the review of this article.

Abstract—Right ventricular (RV) dysfunction is known to be highly correlated with mortality and morbidity; nevertheless, imaging-based assessment of RV anatomy and physiology lags far behind that of the left ventricle. In this study, we advance RV imaging using cardiac magnetic resonance (CMR) to accomplish the following aims: (i) track the motion of six tricuspid annular (TA) sites using a semi-automatic tracking system; (ii) extract clinically important TA measurements—systolic velocity (Sm), early diastolic velocity (Em), late diastolic velocity (Am), and TA plane systolic excursion (TAPSE)—for each TA site and compare these CMR-derived measurements in healthy subjects vs. patients with heart failure, repaired tetralogy of Fallot, pulmonary hypertension, and hypertrophic cardiomyopathy; (iii) investigate how the TA motion related measurements compare with information provided by invasive right heart catheterization (RHC); (iv) evaluate the rate of change in surface area swept out by the reconstructed tricuspid annulus over time and (v) assess the reproducibility of this CMR-based technique. Results indicate that TA motion parameter data obtained in three dimensions using the proposed CMR-based systematic methodology achieve superior diagnostic performance (Sm: AUC = 0.957; TAPSE: AUC = 0.981) compared to two-dimensional CMR imaging. Both Sm and TAPSE from CMR correlated positively with dP/dt_{max}/IP from RHC (Sm: $r = 0.621$, $p < 0.01$; TAPSE: $r = 0.648$, $p < 0.01$). Our highly reproducible and robust methodology holds potential for extending CMR imaging to characterization of TA morphology and dynamic behaviour, eventually leading to deeper understanding of RV function and improved diagnostic capability.

Keywords—Right ventricular function, Tricuspid annulus, Cardiac magnetic resonance.

ABBREVIATIONS

3D	Three dimensional
Am	Peak tricuspid annular velocity during atrial contraction
CMR	Cardiac magnetic resonance
EF	Ejection fraction
Em	Peak tricuspid annular velocity during early diastolic filling
HCM	Hypertrophic cardiomyopathy
HF	Heart failure
PH	Pulmonary hypertension
rTOF	Repaired tetralogy of Fallot
RHC	Right heart catheterization
RV	Right ventricular
Sm	Peak tricuspid annular systolic velocity
SSA	Sweep surface area
SSAV	Sweep surface area velocity
TA	Tricuspid annular
TAPSE	Tricuspid annular plane systolic excursion

INTRODUCTION

An understanding of the role of the right ventricle in health and disease has lagged behind that of the left ventricle.[48] Right ventricular (RV) dysfunction is associated with increased morbidity and mortality in patients with pulmonary hypertension (PH), congenital heart disease (CHD), coronary artery disease

Address correspondence to Ben He, Department of Cardiology, Renji Hospital, School of Medicine, Shanghai Jiaotong University, Shanghai 200001, People's Republic of China. Liang Zhong, National Heart Centre Singapore, 5 Hospital Drive, Singapore 169609, Singapore. Electronic mails: heben@medmail.com.cn and zhong.liang@nhcs.com.sg

Co-first authors Shuang Leng and Meng Jiang have equally contributed to this work.

(CAD), heart failure (HF), and valvular heart diseases.[17,20,22,32] Moreover, RV dysfunction may also affect left ventricular (LV) function, not only by limiting LV preload, but also by adverse systolic and diastolic interaction *via* the intraventricular septum and the pericardium.[6] Thus, the need for diagnosis of RV dysfunction is highly evident. Accurate evaluation of RV function remains challenging, however, due to the complicated geometry and extreme sensitivity to loading conditions. At present, there is no widely accepted or generally applicable index of RV function.[19]

Right heart catheterization (RHC) remains the gold standard for assessment of RV function, but this requires an invasive procedure. In clinical practice, echocardiography is the main diagnostic modality for RV structure and function. Several echocardiography-derived indices, such as peak systolic and diastolic velocities of tricuspid annular (TA) motion, TA plane systolic excursion (TAPSE), and RV index of myocardial performance have emerged as promising parameters of RV function.[21] Transthoracic echocardiography measurements have limitations, however, due to variability in sampling locations and ultrasound beam alignment. Very small changes in beam angle and changes in imaging window can result in dramatically different conclusions about RV size and function.[19] Three-dimensional (3D) echocardiography is one of several emerging modalities for defining cardiac anatomy and function. Available evidence suggests that 3D echocardiography provides better accuracy over two-dimensional (2D) methods for evaluation of LV volume and function.[15] There are still certain limitations to currently available 3D ultrasound methods, however, even with state-of-the-art real-time 3D echocardiography systems. In particular, relatively low image quality and low frame rate may limit everyday clinical use of 3D echocardiography.[44]

Cardiac magnetic resonance (CMR) has been an alternative non-invasive modality of choice for quantitatively assessing RV volume and regional area strain.[8,50] CMR-based measurements of RV ejection fraction (EF) are strong predictors of clinical outcome over a wide range of HF severity.[13] Very few studies have been undertaken, however, to quantify the motion of tricuspid annulus for RV function assessment using CMR imaging. In Nijveldt *et al.*,[36] the TAPSE and RV fractional shortening were manually evaluated in CMR and compared with volumetric assessment of RV function. Another approach used the modelling technique to measure TAPSE at the junction of RV free wall and tricuspid annulus in the apical four-chamber CMR view.[31] In Ito *et al.*,[23] the position of the RV atrioventricular junction (AVJ) was tracked in all CMR images and projected onto a reference line, bisecting the right ventricle between the RV apex and the free wall. The displacement of the RV AVJ along the reference line was measured relative to the position at end-diastole (ED) phase. The RV long-axis displacement has also been estimated by tagging CMR which demonstrated more significant differences between the studied groups than did RVEF.[9]

Despite some recent advances, the 3D assessment of TA motion with CMR remains challenging predominantly due to a paucity of automatic, robust and time-efficient CMR-based methods. Accordingly, the goals of the present study were as follows: (i) To introduce a novel CMR-based systematic tool and methodology for 3D TA motion assessment with multiple CMR planes, (ii) To semi-automatically track six TA points from the four-chamber, RV three-chamber, and RV two-chamber views with CMR imaging in healthy subjects and patients with HF, repaired tetralogy of Fallot (rTOF), PH, and hypertrophic cardiomyopathy (HCM) using developed system, (iii) To investigate how TA motion related measurements compare with information provided by invasive RHC, (iv) To quantify the rate of change in surface area swept out by the reconstructed tricuspid annulus at successive times, and (v) To evaluate reproducibility of the technique.

MATERIALS AND METHODS

Study Population

A group of thirty-eight subjects was enrolled and underwent CMR scan, including 16 normal subjects, 6 patients with HF, 5 patients with rTOF, 5 patients with PH, and 6 patients with HCM. None of the normal subjects had significant valvular or congenital cardiac diseases, or history of cardiovascular symptoms.

In addition, another group of fifteen patients with PH (38 ± 18.4 years, 11 females) who had clinical indication for RHC were consecutively selected and underwent both CMR and RHC within a span of 7 days.

The protocol was approved by the Local Institutional Review Board, and informed consent was obtained from each participant.

CMR Acquisition

CMR scans were performed using balanced turbo field echo sequence (BTFE). All subjects were imaged on a 3T magnetic resonance imaging (MRI) system (Ingenia, Philips Healthcare, The Netherlands) with a dStream Torso coil (maximal number of channels 32). BTFE end-expiratory breath hold cine images were acquired in multiplanar long-axis views (namely *four-chamber*, *RV three-chamber*, and *RV two-chamber* views, as indicated in Fig. 1). The RV two-chamber view was piloted by bisecting the right ventricle in the four-chamber view (slice through tricuspid valve and RV apex). The RV three-chamber (RV inflow/outflow) view was piloted by 3

points: centre of pulmonary valve in RV outflow tract (RVOT) view, centre of tricuspid valve on RV four-chamber or two-chamber view, and apex on RV four-chamber or two-chamber view. The following typical sequence parameters were used: TR/TE 3/1 ms, flip angle 45°, slice thickness 8 mm for both short- and long-axis, pixel bandwidth 1797 Hz, field of view 280–450 mm, temporal resolution ≈28 ms, in plane spatial resolution 0.6 mm × 0.6 mm–1.1 mm × 1.1 mm, frame rate was selected as 30 or 40 frames per cardiac cycle.

Right Heart Catheterization

RHC was performed at rest using standard techniques for continuous measurement of RV chamber pressure. The RV pressure was then differentiated with respect to time for determination of maximal rate of increase during systole (RV dP/dt_{max}). The RV dP/dt_{max} was normalized to instantaneous pressure (IP) at which dP/dt_{max} occurred (dP/dt_{max}/IP). Peak ECG R wave was used as the end-diastolic timing marker.

Overall Methodology Framework

Figure 2 provides the flowchart of the methodology employed in our study for assessing 3D TA motion. The CMR imaging sequences were acquired in clinical practice and conformed to the DICOM protocol. The following meta-information was recorded for all image sequences: *trigger time*, *image position* (3-by-1 vector denoted by **ImagePos**), *image orientation* along horizontal (3-by-1 vector denoted by $\mathbf{ImageOri}_h$) and vertical (3-by-1 vector denoted by $\mathbf{ImageOri}_v$) directions, and *pixel spacing*. Our own program, developed in-house, was applied to locate TA points throughout the cardiac cycle in multiple CMR planes. Peak velocities and maximal displacements at multiple TA points were extracted and interpreted. Alternatively, the 3D tricuspid annulus was reconstructed as a function of time by 2D projection and interpolation with the TA tracking results. Sweep surface area velocity, a new diagnostic marker, was calculated and analyzed. Detailed discussions on each step are given in the following subsections.

Semi-automatic TA Tracking in Multiple CMR Planes

Custom software, developed in the MATLAB environment (MathWorks Inc., MA, USA), was used to perform the semi-automatic tracking of TA motion in multiple CMR planes. Specifically, in this study, 6 different TA points were tracked (Fig. 1): the RV septal and lateral sites (obtained from the apical

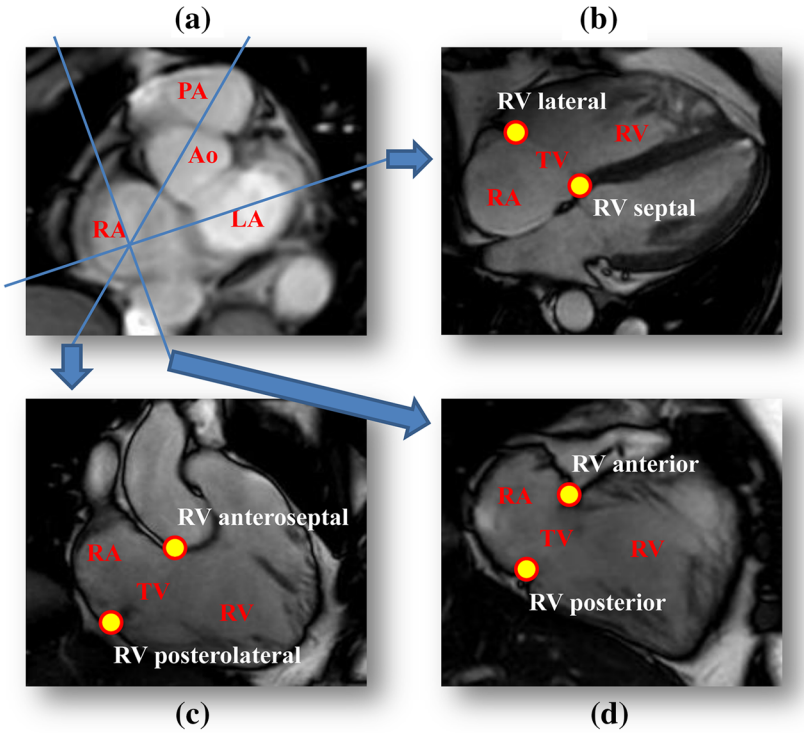

FIGURE 1. CMR acquisition: (a) short-axis view (b) long-axis four-chamber view (c) long-axis right ventricular (RV) three-chamber view (d) long-axis RV two-chamber view. Solid lines in (a) denote cutting planes through which long-axis views are obtained. Motion of 6 TA points are assessed: RV septal and lateral (in four-chamber view), RV anteroseptal and posterolateral sites (in RV three-chamber view), and RV anterior and posterior sites (in RV two-chamber view). RA: right atrium; LA: left atrium; Ao: aorta; PA: pulmonary artery; RV: right ventricle; TV: tricuspid valve.

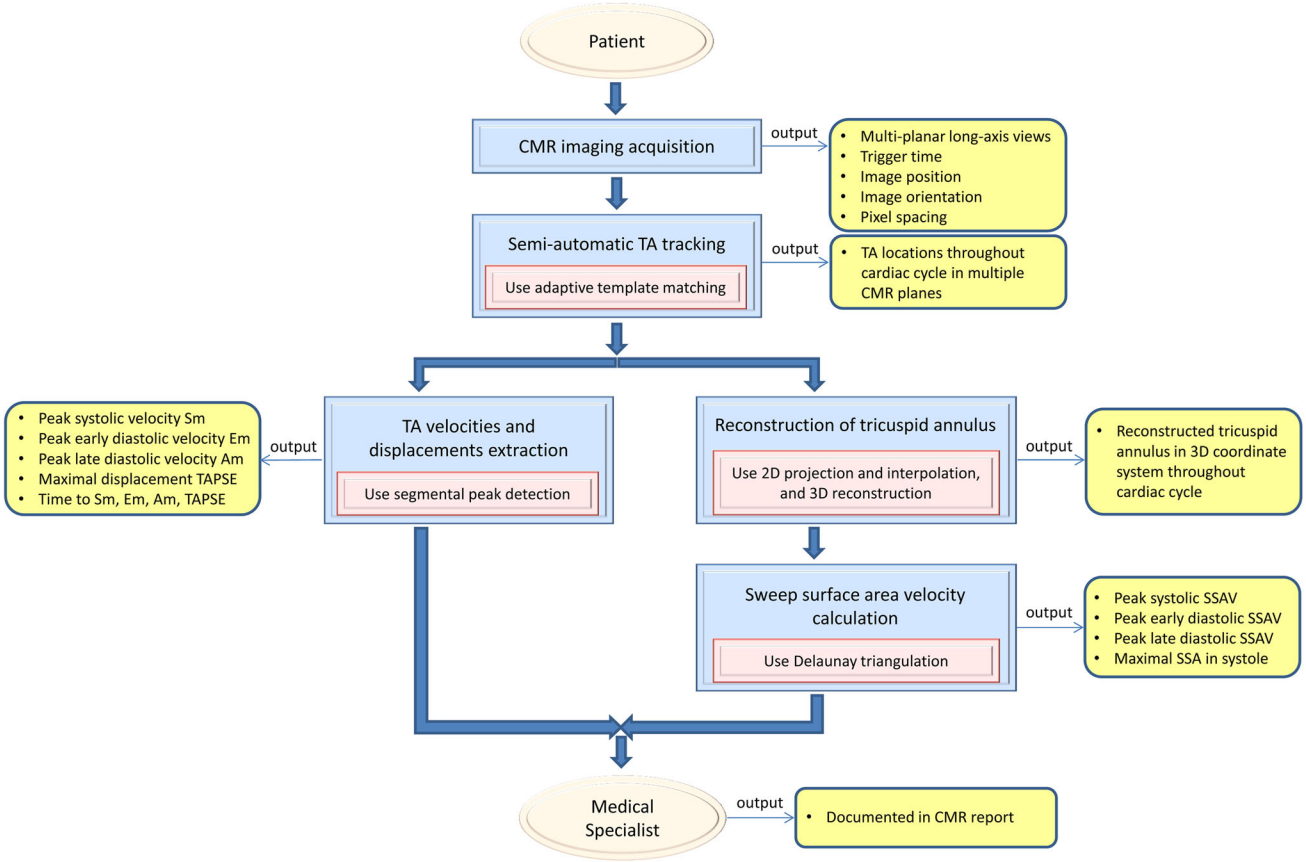

FIGURE 2. Flowchart of the present method for 3D TA motion assessment.

four-chamber view), the RV anteroseptal and posterolateral sites (obtained from the apical RV three-chamber view), and the RV anterior and posterior sites (obtained from the apical RV two-chamber view).

The tracking system used the method of template matching,[18] which is an algorithm for searching and finding the location of a template image within a larger image (called the search region). Figure 3 outlines the procedure of applying adaptive template matching in TA tracking with CMR imaging. The user selected the template with size $(2w + 1) \times (2h + 1)$ in ED frame of a CMR imaging sequence (usually frame 1 as shown by read solid rectangle in Fig. 3a) by visual inspection. Typical values of selected w and h ranged from 8-10 pixels. The search region sharing the same centre with the selected template was automatically generated in frame 2 with size $(2w + 1 + 2l) \times (2h + 1 + 2l)$ where l denotes the length of the searched neighbourhood (blue dash rectangle in Fig. 3a). The value of l (set to be 10 pixels in this study) was selected such that the maximal displacement between TA points in successive frames was close to but smaller than l. The template matching was conducted to detect the best match of the template in the search region by sliding the template image over the search image one pixel at a time (left to right, up to down) while computing the normalized cross correlation at each location. The point with the highest correlation coefficient in the resulting correlation image (Fig. 3b) indicated the location of the best match. This point was used to update the template in frame 2 that underwent the same template matching within the automatically extracted search region in frame 3 (Fig. 3c). This same procedure was automatically executed iteratively for all subsequent frames.

CMR TA Velocity and Displacement Extraction

TA velocity curves were generated by dividing the CMR effective image acquisition time by the Euclidean distance between tracked template positions on two adjacent frames (Fig. 4, middle column). TA displacement curves were then obtained as the cumulative integrals of TA velocity over the cardiac cycle, using the trapezoidal rule (Fig. 4, right column). At each of the 6 TA sites, 3 peak velocities were automatically extracted in systole, and in early and late diastole using segmental peak detection (Fig. 4, middle column). These were (i) positive peak systolic velocity as the tricuspid annulus descends toward the RV apex (Sm), (ii) early diastolic velocity below the baseline as the

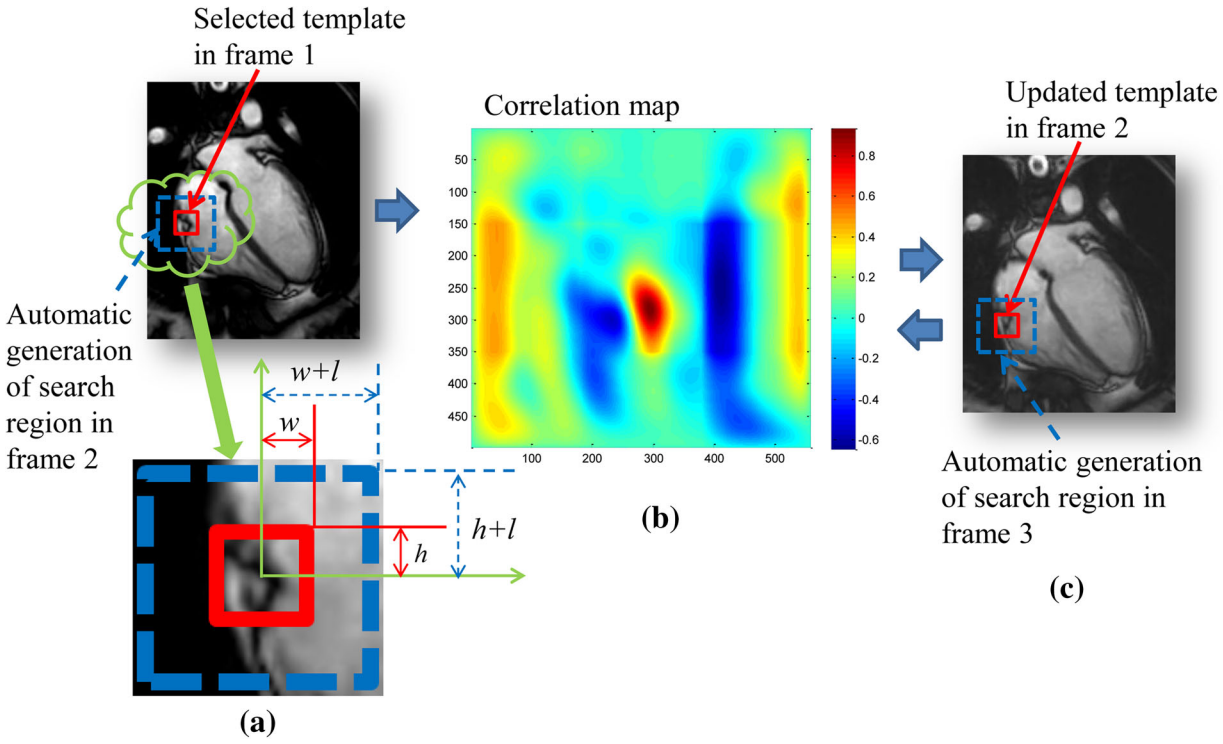

FIGURE 3. Workflow of the TA tracking system: (a) Selected mask in frame 1 and automatically generated search region in frame 2, (b) correlation map, and (c) automatically updated mask in frame 2 and search region in frame 3.

tricuspid annulus ascends away from the RV apex (Em), and (iii) late diastolic velocity during right atrial contraction (Am). Maximal displacement (TAPSE) in ventricular systole was determined from the TA displacement curve (Fig. 4, right column). In addition, time to Sm, Em, Am and TAPSE (denoted T-Sm, T-Em, T-Am and T-TAPSE) were recorded and used to calculate RV peak velocity and displacement dyssynchrony indices, defined as the standard deviation (SD) of time to peak velocity and SD of time to maximal displacement, respectively, among the 6 TA points.

Reconstruction of Tricuspid Annulus

The semi-automatic tracking system provided spatial coordinates of multiple points located on the tricuspid annulus as a function of CMR frame time. Reconstruction of the tricuspid annulus was accomplished in 4 steps:

(1) The 2D spatial coordinates of each of the 6 TA points (e.g., frame 1 shown in Fig. 5a) were mapped into a 3D coordinate system with respective image position and image orientation information using the transformation:

$$\mathbf{Coord}_{3D} = Coord_{2D,x} \times \mathbf{ImageOri}_h + Coord_{2D,y} \times \mathbf{ImageOri}_v + \mathbf{ImagePos} \quad (1)$$

where $\mathbf{Coord}_{3D}$ represents the 3-by-1 coordinate vector in 3D space, scalars $\mathbf{Coord}_{2D,x}$ and $\mathbf{Coord}_{2D,y}$ are 2D coordinates in x- and y-axis, $\mathbf{ImageOri}_h$ and $\mathbf{ImageOri}_v$ are the 3-by-1 image orientation vectors along horizontal and vertical directions, and **ImagePos** denotes the 3-by-1 image position vector.

(2) The mapped 3D coordinates $\mathbf{Coord}_{3D}$ were projected onto a new 2D Cartesian coordinate plane defined by the centroid of the mapped coordinates and two points in the 3D coordinate system.

(3) A curve was generated in the 2D Cartesian plane by interpolating the projected coordinates using piecewise cubic Hermite interpolation.[28]

(4) The tricuspid annulus was reconstructed by inverse projection of the curve back onto the 3D coordinate system (reconstructed tricuspid annulus at cardiac frame 1 shown in Fig. 5b).

The same procedure was applied for TA reconstruction at each cardiac frame and Fig. 5c shows the results for frames 1, 3, 5, 7, 9, and 11, respectively.

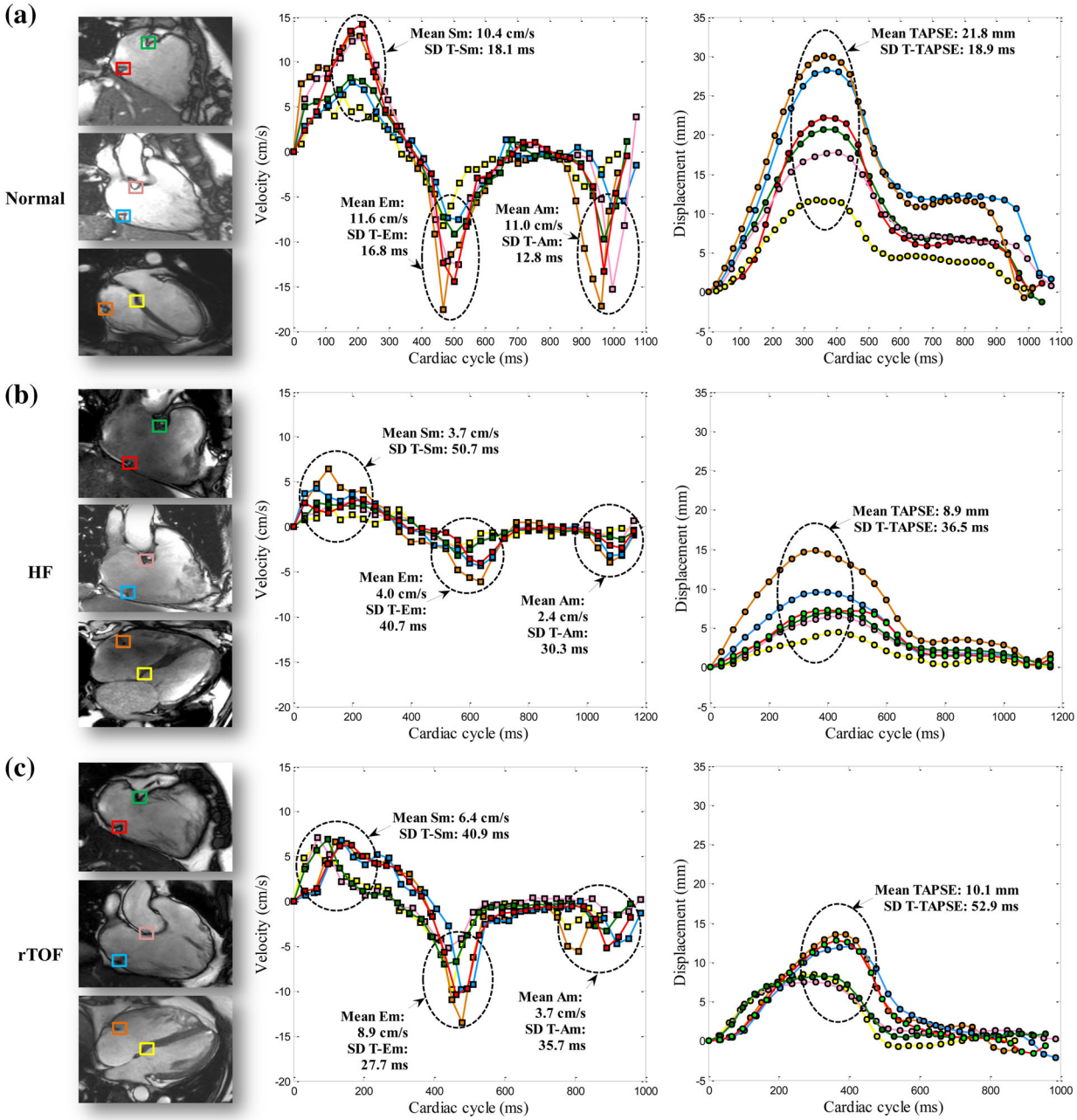

FIGURE 4. Representative examples of generating velocity (middle column) and displacement (right column) curves at 6 TA sites (indicated with rectangles in left column) and extracting motion parameters in (a) 44-year-old female healthy volunteer, (b) 51-year-old male HF patient, and (c) 19-year-old male rTOF patient. Parameters include 6-point mean Sm, Em, Am, TAPSE, and standard deviations of T-Sm, T-Em, T-Am, T-TAPSE.

TA Sweep Surface Area Velocity

Two new CMR-based indices, sweep surface area (SSA) and sweep surface area velocity (SSAV), are proposed and adopted in the present study to further quantitatively characterize 3D TA motion. Following the TA reconstruction by a curve representing the boundary of the tricuspid annulus at each CMR frame (Fig. 5c), the SSA (area bounded between the corresponding curves) was computed as the surface area swept out by the tricuspid annulus at successive CMR frames (illustration in Fig. 5d) by Delaunay triangulation.[12] The rate of TA motion was then quantified using SSAV by taking the first order time derivative of SSA. Parameters extracted from the resulting SSAV and SSA curves (Figs. 5e and 5f) were: positive peak systolic SSAV (S_{SSAV}), negative peak early diastolic

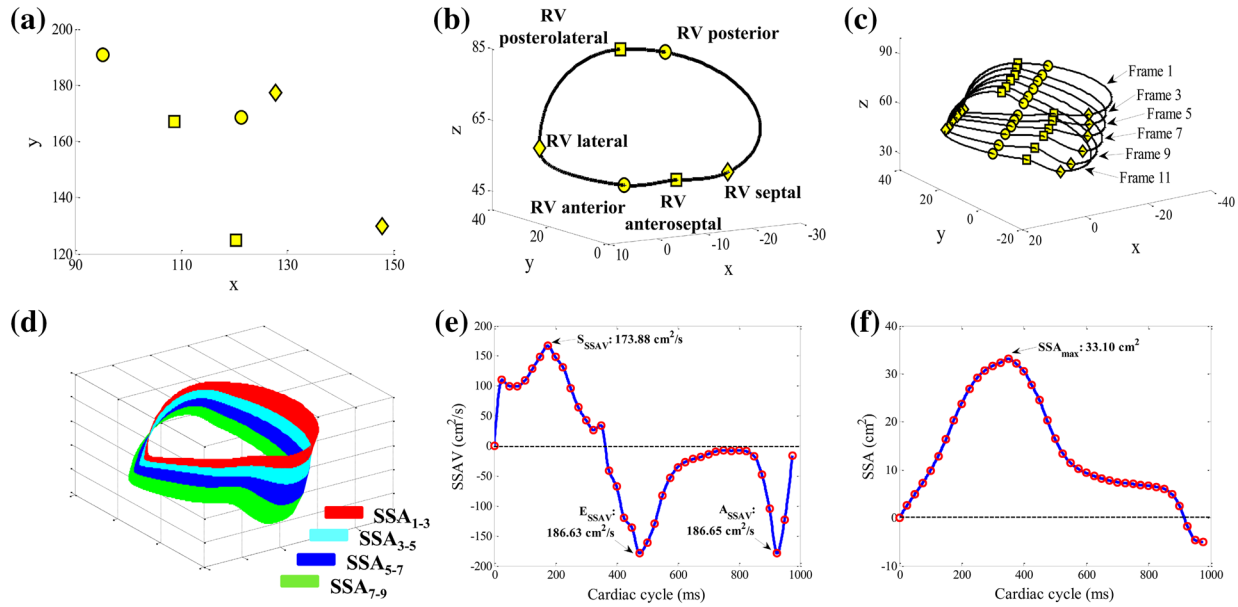

FIGURE 5. Reconstruction of 3D tricuspid annulus and extraction of SSA and SSAV in a 34-year-old female healthy volunteer: (a) TA points in 2D coordinate system at cardiac frame 1. (b) 3D reconstruction of tricuspid annulus at cardiac frame 1. (c) Reconstructed tricuspid annulus at cardiac frames 1, 3, 5, 7, 9, and 11. (d) Indicative illustration of sweep surface area calculation, SSA_{1-3}: SSA from frame 1 to 3, SSA_{3-5}: SSA from frame 3 to 5, *etc.* (e) SSAV curve and extracted peak SSAV values. (f) SSA curve and extracted maximal SSA value.

SSAV (E_{SSAV}), negative peak late diastolic SSAV (A_{SSAV}), and maximal SSA (SSA_{max}) in systole.

Statistical Analysis

Data was analyzed using SPSS (version 17.0, Chicago, IL, USA) and SAS (version 9.3, Cary, NC, USA). Comparisons of demographics, patient characteristics, and CMR measurements between patients and control subjects were performed using independent *t* tests for normally distributed data, Mann–Whitney *U* tests for non-normally distributed data, and Fisher's exact test for categorical data. Mean age differed substantially among some study groups, which might influence cardiac function measurements. Therefore, each CMR-based TA motion parameter was adjusted for age using one-way analysis of covariance. An *F* test was used to test the omnibus hypothesis of equality among diagnosis groups of age-adjusted least-squares means, which was then followed up with post hoc comparisons of HF, rTOF, PH and HCM age-adjusted means to the normal mean. A p value <0.05 was considered statistically significant.

Intra- and inter-observer variability in CMR-derived TA velocities was assessed by Pearson's *r* correlation, Bland–Altman analysis and intra-class correlation coefficient (ICC) using data from 6 randomly chosen subjects (2 normal controls, 2 HF patients and 2 rTOF patients). Inter-observer variability was assessed by comparing measurements made by two independent observers. Intra-observer variability was assessed from repeated measurements, 3 days apart, on the same 6 cases by the same observer.

RESULTS

Patient Demographics

Baseline demographic and clinical characteristics of enrolled subjects are summarized in Table 1. HF patients had significantly lower LVEF and LV stroke volume (SV) and higher LV end-diastolic volume (EDV), LV end-systolic volume (ESV) and LV mass compared to normal controls. Significant RV dilation in rTOF patients was indicated on CMR by large values of RVEDV, RVESV and RVSV. PH patients had significantly higher RVEDV and RVESV. Patients with HF, rTOF, and PH exhibited significantly reduced RVEF compared to controls.

TA Tracking and Motion Parameters Extraction

Semi-automatic TA tracking required approximately 3 min per subject (6 TA points), including initialization, tracking and motion parameter extraction. Velocity and displacement curves were obtained for all subjects.

A representative example of TA tracking results for a four-chamber view in a 44-year-old female healthy volunteer is shown in Fig. 6 at start-of-systole, end-systole (ES), diastasis, and ED. Velocity and

TABLE 1. Baseline demographic and clinical characteristics of study subjects.

Variables	Patient diagnosis group					
	Normal ($n = 16$)	HF ($n = 6$)	rTOF ($n = 5$)	PH ($n = 5$)	HCM ($n = 6$)	p value (ANOVA)
Male/female	6/10	6/0	4/1	1/4	4/2	0.0196[a]
Age (years)	49.9 ± 15.2	58.0 ± 9.0	30.0 ± 13.4*	47.0 ± 10.7	55.7 ± 13.4	0.0154
BSA (m^2)	1.8 ± 0.3	1.8 ± 0.1	1.9 ± 0.4	1.8 ± 0.1	1.8 ± 0.2	0.8679
Height (cm)	164.1 ± 9.3	172.2 ± 6.9	167.6 ± 10.0	159.4 ± 5.7	168.3 ± 8.2	0.0581
Weight (kg)	67.2 ± 19.4	69.4 ± 5.7	78.4 ± 26.6	68.9 ± 7.1	67.0 ± 10.8	0.4413
DP (mmHg)	83.9 ± 13.6	73.2 ± 10.0	78.7 ± 10.7	81.8 ± 12.0	74.7 ± 6.7	0.2925
SP (mmHg)	128.8 ± 17.5	111.8 ± 15.9*	146.0 ± 23.8	131.2 ± 12.7	127.0 ± 20.4	0.1090
LV EDV index (ml $m^{2\ -1}$)	69.2 ± 21.4	172.4 ± 42.4*	80.3 ± 13.1	36.5 ± 12.0*	51.3 ± 7.5	<0.0001
LV ESV index (ml $m^{2\ -1}$)	24.4 ± 16.0	139.4 ± 36.6*	34.9 ± 8.6*	13.7 ± 7.1	12.4 ± 2.5*	<0.0001
LV SV index (ml $m^{2\ -1}$)	44.9 ± 12.1	32.8 ± 11.3*	45.2 ± 10.6	22.9 ± 5.6*	38.9 ± 7.1	0.0026
LV EF (%)	66.3 ± 10.5	18.9 ± 5.1*	56.4 ± 8.0*	64.8 ± 8.7	75.7 ± 5.2*	<0.0001
LV Mass index (g $m^{2\ -1}$)	69.9 ± 27.6	115.9 ± 25.0*	55.5 ± 9.4	52.3 ± 6.4*	89.0 ± 18.7*	0.0001
RV EDV index (ml $m^{2\ -1}$)	58.1 ± 20.4	94.2 ± 34.2*	148.4 ± 19.8*	92.2 ± 39.4*	41.7 ± 10.1	<0.0001
RV ESV index (ml $m^{2\ -1}$)	25.1 ± 11.0	62.4 ± 32.0*	82.1 ± 11.1*	59.1 ± 22.8*	14.2 ± 4.1*	<0.0001
RV SV index (ml $m^{2\ -1}$)	33.0 ± 13.7	31.8 ± 5.4	66.3 ± 11.7*	33.1 ± 17.0	27.5 ± 8.2	<0.0001
RV EF (%)	57.4 ± 11.9	37.0 ± 13.4*	44.4 ± 4.0*	34.8 ± 4.0*	65.8 ± 8.5	<0.0001

Data are represented as mean ± SD. BSA: body surface area; DP: diastolic pressure; SP: systolic pressure; LV: left ventricular; EDV: end-diastolic volume; ESV: end-systolic volume; SV: stroke volume; EF: ejection fraction; RV: right ventricular; HF: heart failure; rTOF: repaired tetralogy of Fallot; PH: pulmonary hypertension; HCM: hypertrophic cardiomyopathy.

[a]Fisher's exact test.

* Statistically significant difference between normal controls and patients ($p < 0.05$).

displacement curves at 6 TA sites are shown in Fig. 4a. Three peaks (one positive and two negative) are present for each velocity curve and correspond to the peak velocities during systole (Sm), early diastolic rapid filling (Em), and late diastolic atrial contraction (Am). The extracted values of 6-point mean Sm, Em and Am were 10.4, 11.6, and 11.0 cm s^{-1}, respectively. The mean value for TAPSE derived from the displacement curves was 21.8 mm. The respective SDs for times to peak velocity and displacement (SD T-Sm, SD T-Em, SD T-Am and SD T-TAPSE) were 18.1, 16.8, 12.8 and 18.9 ms. Moreover, one can observe that the tricuspid annulus is nearly stationary during the diastolic slow filling phase as indicated by a zone of very low velocity and constant displacement. Figures 4b and 4c show results for a 51-year-old male HF patient and a 19-year-old male rTOF patient.

TA Motion Parameters Among Patients And Controls

Table 2 gives the 3D CMR-derived motion parameters with differentiation by subject group. The 6-point mean results show that patients with HF and PH had significantly reduced Sm (4.2 ± 1.3/5.0 ± 1.0 vs. 9.7 ± 1.7 cm s^{-1}, $p < 0.05$), Em (3.4 ± 1.0/3.7 ± 1.0 vs. 8.3 ± 3.0 cm s^{-1}, $p < 0.05$), Am (4.3 ± 2.4/6.0 ± 2.1 vs. 10.1 ± 2.6 cm s^{-1}, $p < 0.05$) and TAPSE (7.9 ± 2.7/8.8 ± 1.8 vs. 17.6 ± 2.4 mm, $p < 0.05$) and significantly larger SD for time to TAPSE (51.3 ± 19.7/84.3 ± 20.3 vs. 24.1 ± 6.0 ms, $p < 0.05$) in comparison with normal controls.

The group of rTOF patients exhibited significantly lower 6-point mean Sm (7.5 ± 1.1 vs. 9.7 ± 1.7 cm s^{-1}, $p < 0.05$), Am (6.6 ± 2.1 vs. 10.1 ± 2.6 cm s^{-1}, $p < 0.05$) and TAPSE (13.6 ± 2.3 vs. 17.6 ± 2.4 mm, $p < 0.05$) compared to normal controls.

Patients with HCM had comparable Sm (9.5 ± 1.9 vs. 9.7 ± 1.7 cm s^{-1}, $p = 0.846$) but relatively lower Em (6.1 ± 0.8 vs. 8.3 ± 3.0 cm s^{-1}, $p = 0.062$) and Am (8.3 ± 1.1 vs. 10.1 ± 2.6 cm s^{-1}, $p = 0.137$) compared to those in the control group.

CMR Derived Sm, TAPSE and RVEF

Good overall correlation was found between CMR-derived 6-point average peak systolic TA velocity Sm and RVEF (Fig. 7a, $r = 0.675$ $p < 0.01$) and between the CMR-derived 6-point mean TAPSE and RVEF (Fig. 7b, $r = 0.651$, $p < 0.01$). The utility of CMR-based measurements for diagnosing disease states (HF, rTOF and PH) vs. normal controls is demonstrated in Table 3, where area under the receiver-operating characteristic (ROC) curve (AUC) for the CMR-based 6-point mean Sm and TAPSE, and RVEF were 0.957, 0.981 and 0.871, respectively.

CMR Derived Sm, TAPSE vs. RHC Derived dP/dt_{max}/IP

The CMR-derived Sm and TAPSE in the patient cohort with PH were based on an average of 4 TA points, since only four-chamber and RV two-chamber CMR

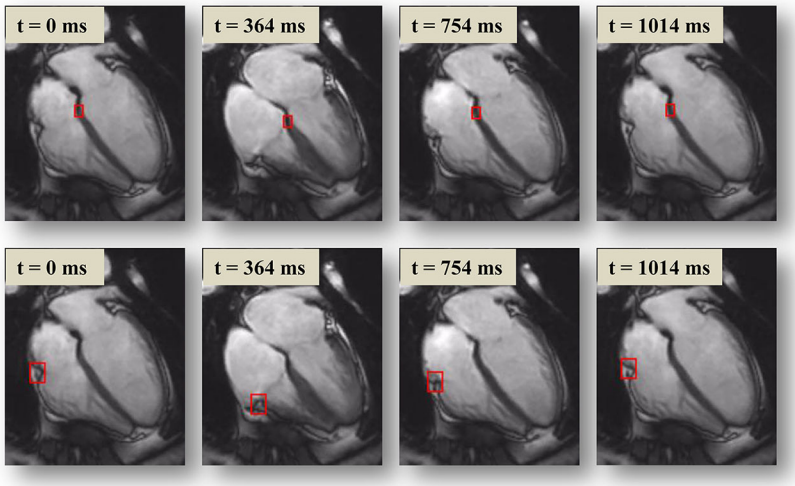

FIGURE 6. TA tracking results for a 44-year-old female healthy volunteer: (top) RV septal (bottom) RV lateral, templates indicated by red rectangles.

TABLE 2. Average CMR-derived motion parameters based on 3D results.

		Patient diagnosis group								
3D TA motion parameter	*F*-test *p* value[$]	Normal ($n = 16$)	HF ($n = 6$)	HF vs. normal *p* value[$]	rTOF ($n = 5$)	rTOF vs. normal *p* value[$]	PH ($n = 5$)	PH vs. normal *p* value[$]	HCM ($n = 6$)	HCM vs. normal *p* value[$]
Sm (cm s^{-1})	<0.0001	9.7 ± 1.7	4.2 ± 1.3	<0.0001	7.5 ± 1.1	0.0043	5.0 ± 1.0	<0.0001	9.5 ± 1.9	0.8463
Em (cm s^{-1})	<0.0001	8.3 ± 3.0	3.4 ± 1.0	<0.0001	9.0 ± 1.3	0.5049	3.7 ± 1.0	<0.0001	6.1 ± 0.8	0.0618
Am (cm s^{-1})	<0.0001	10.1 ± 2.6	4.3 ± 2.4	<0.0001	6.6 ± 2.1	0.0036	6.0 ± 2.1	0.0011	8.3 ± 1.1	0.1366
Em/Am	0.1798	0.8 ± 0.3	1.4 ± 1.6	0.0823	1.5 ± 0.6	0.1376	0.7 ± 0.3	0.7518	0.7 ± 0.1	0.8567
TAPSE (mm)	<0.0001	17.6 ± 2.4	7.9 ± 2.7	<0.0001	13.6 ± 2.3	0.0022	8.8 ± 1.8	<0.0001	16.2 ± 2.6	0.3239
T-Sm (ms)	0.0950	118.9 ± 33.0	131.3 ± 35.9	0.2027	126.4 ± 31.2	0.6316	142.2 ± 30.2	0.1752	92.1 ± 15.9	0.1283
T-Em (ms)	0.7414	511.2 ± 51.4	538.9 ± 13.7	0.2282	497.8 ± 29.4	0.7641	516.2 ± 45.1	0.7854	510.2 ± 29.4	0.8946
T-Am (ms)	0.2518	806.7 ± 87.2	822.7 ± 108.3	0.8738	841.8 ± 72.1	0.2131	761.3 ± 38.0	0.3451	868.5 ± 76.1	0.1796
T-TAPSE (ms)	0.0294	376.5 ± 41.3	380.7 ± 21.0	0.6933	369.7 ± 37.4	0.5105	437.7 ± 29.6	0.0035	390.6 ± 40.0	0.3713
SD T-Sm (ms)	0.0067	17.9 ± 9.2	42.3 ± 25.0	0.0016	34.6 ± 13.4	0.0916	41.5 ± 15.7	0.0099	24.0 ± 10.5	0.3756
SD T-Em (ms)	0.0380	21.6 ± 9.1	37.9 ± 21.5	0.0286	26.2 ± 6.2	0.8045	48.7 ± 38.6	0.0144	26.7 ± 7.1	0.4288
SD T-Am (ms)	0.0756	21.2 ± 7.8	27.9 ± 8.7	0.0562	28.9 ± 11.9	0.4680	25.7 ± 1.3	0.1211	21.7 ± 6.2	0.7815
SD T-TAPSE (ms)	<0.0001	24.1 ± 6.0	51.3 ± 19.7	0.0006	39.1 ± 19.2	0.1200	84.3 ± 20.3	<0.0001	27.3 ± 14.3	0.6548

Values are mean ± SD. CMR: cardiac magnetic resonance; TA: tricuspid annular; Sm: peak TA systolic velocity; Em: peak TA velocity during early diastolic filling; Am: peak TA velocity during atrial contraction; TAPSE: maximal displacement; T-Sm: time to Sm; T-Em: time to Em; T-Am: time to Am; T-TAPSE: time to TAPSE; SD: standard deviation; HF: heart failure; rTOF: repaired tetralogy of Fallot; PH: pulmonary hypertension; HCM: hypertrophic cardiomyopathy.
[$] Adjusted for age.

images were available for this group of patients. As presented in Figs. 7c and 7d, both Sm and TAPSE from CMR correlated positively with dP/dt_{max}/IP from RHC (Sm: $r = 0.621, p < 0.01$; TAPSE: $r = 0.648, p < 0.01$).

CMR Derived SSA and SSAV

Figures 5e and 5f show the SSAV and SSA curves for a 34-year-old female healthy volunteer. The extracted global values of S_{SSAV}, E_{SSAV}, A_{SSAV}, and SSA_{max} were 173.9, 186.6, 186.7 cm^2 s^{-1}, and 33.1 cm^2, respectively. Figure 8 presents a side-by-side comparison of 2 normal subjects, 2 HF patients and 1 rTOF patient.

The CMR derived peak SSAV and maximal SSA values for each subject group presented in Table 4 indicate that patients with HF had significantly lower S_{SSAV} (53.6 ± 13.1 vs. 129.7 ± 44.2 cm^2 s^{-1}, $p < 0.05$), E_{SSAV} (49.9 ± 13.5 vs. 129.1 ± 54.2 cm^2 s^{-1}, $p < 0.05$), A_{SSAV} (59.7 ± 35.4 vs. 157.3 ±

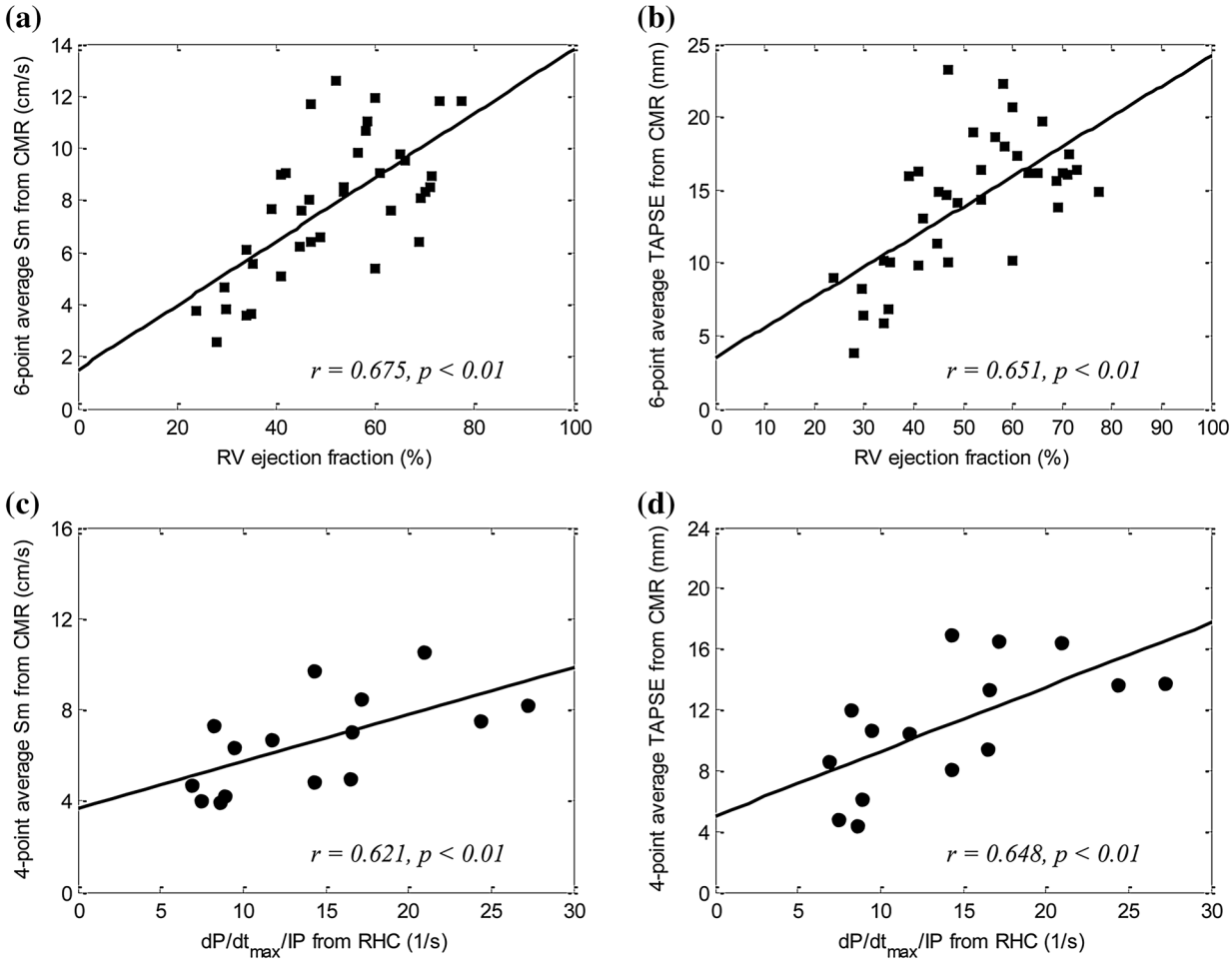

FIGURE 7. Scatterplot with linear regression line demonstrating the relationship of (a) CMR-based mean Sm and RVEF (b) CMR-based mean TAPSE and RVEF (c) CMR-based mean Sm and *dP/dt*$_{max}$/IP from RHC (d) CMR-based mean TAPSE and *dP/dt*$_{max}$/IP from RHC.

TABLE 3. Results of sensitivity, specificity and AUC using CMR-based measurements.

Motion parameters	TA position	Cut-off value	Sensitivity	Specificity	AUC
Sm	RV anterior	7.4 cm s^{-1}	0.929	0.800	0.938
	RV posterior	6.9 cm s^{-1}	0.714	1.000	0.895
	RV anteroseptal	6.1 cm s^{-1}	0.786	0.933	0.929
	RV posterolateral	8.5 cm s^{-1}	0.786	0.800	0.843
	RV septal	4.8 cm s^{-1}	0.714	0.933	0.881
	RV lateral	9.8 cm s^{-1}	0.857	0.867	0.938
	6-point mean	7.8 cm s^{-1}	0.929	0.933	0.957
TAPSE	RV anterior	14.6 mm	0.929	0.867	0.957
	RV posterior	13.8 mm	0.714	0.933	0.848
	RV anteroseptal	10.1 mm	0.857	1.000	0.971
	RV posterolateral	17.6 mm	0.857	0.800	0.886
	RV septal	8.7 mm	0.786	0.733	0.819
	RV lateral	17.0 mm	0.857	1.000	0.971
	6-point mean	15.2 mm	0.929	0.933	0.981
RVEF	–	50.6%	0.929	0.733	0.871

CMR: cardiac magnetic resonance; Sm: peak TA systolic velocity; TAPSE: maximal displacement; TA: tricuspid annular; RV: right ventricular; EF: ejection fraction; AUC: area under the ROC curve.

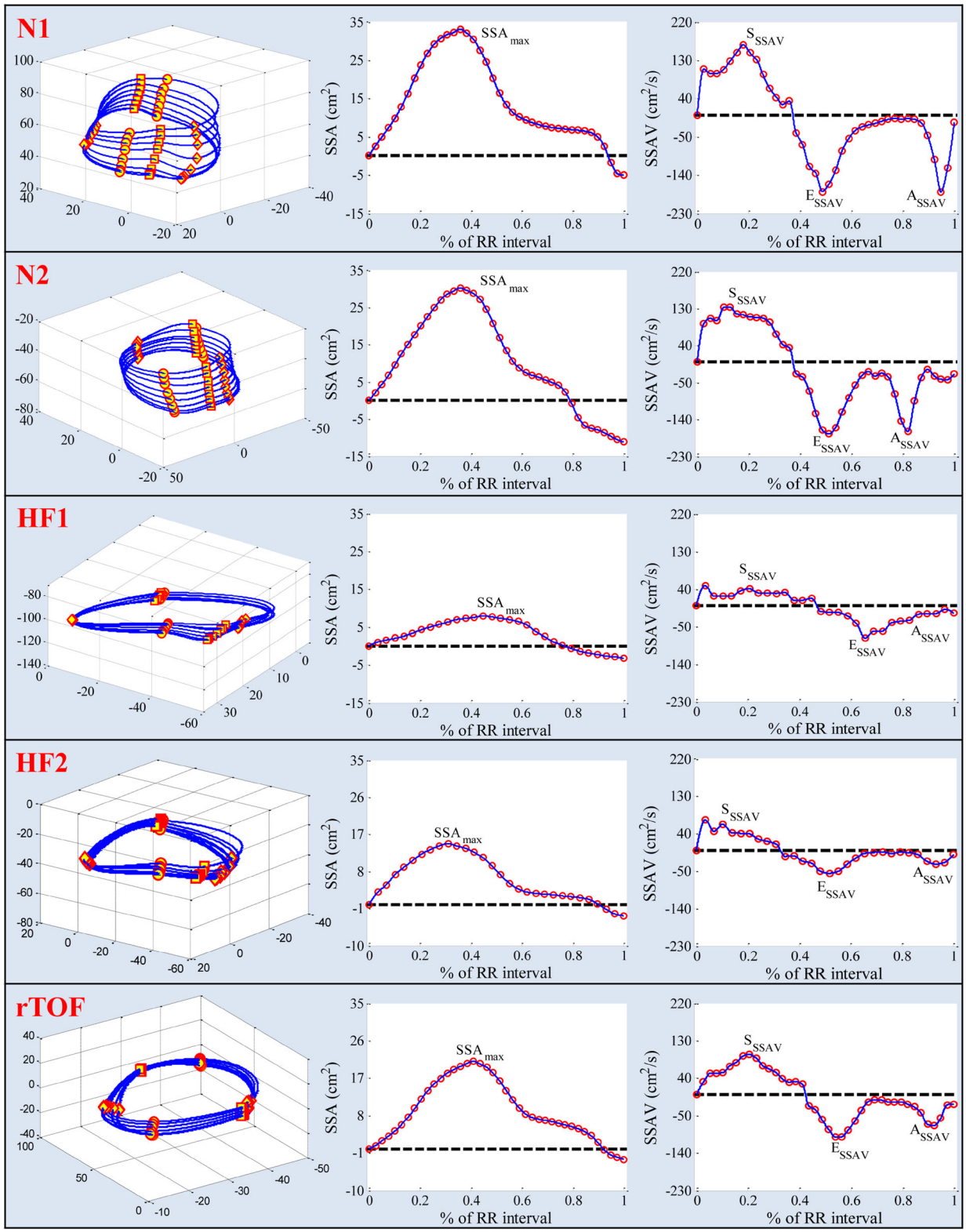

FIGURE 8. 3D TA reconstruction for cardiac frames 1, 3, 5, 7, 9, 11, 13, and 15 (left column), and extraction of SSA_{max} (middle column), S_{SSAV}, E_{SSAV} and A_{SSAV} (right column) in two normal subjects (N1, N2), two HF patients (HF1, HF2) and one rTOF patient (rTOF).

TABLE 4. CMR-derived peak SSAV and maximal SSA.

Motion parameters	*F*-test *p* value[$]	Patient diagnosis group								
		Normal ($n = 16$)	HF ($n = 6$)	HF vs. normal *p* value[$]	rTOF ($n = 5$)	rTOF vs. normal *p* value[$]	PH ($n = 5$)	PH vs. normal *p* value[$]	HCM ($n = 6$)	HCM vs. normal *p* value[$]
S_{SSAV} ($cm^2\ s^{-1}$)	0.002	129.7 ± 44.2	53.6 ± 13.1	0.0023	77.3 ± 21.4	0.0063	55.4 ± 13.9	0.0019	108.9 ± 42.8	0.3079
E_{SSAV} ($cm^2\ s^{-1}$)	0.006	129.1 ± 54.2	49.9 ± 13.5	0.0064	98.7 ± 20.8	0.0406	45.1 ± 20.4	0.0014	88.4 ± 28.9	0.0889
A_{SSAV} ($cm^2\ s^{-1}$)	0.075	157.3 ± 96.2	59.7 ± 35.4	0.0423	71.1 ± 18.4	0.0254	75.9 ± 17.3	0.0610	114.2 ± 18.9	0.3034
E_{SSAV}/A_{SSAV}	0.315	0.89 ± 0.25	1.50 ± 1.60	0.1455	1.46 ± 0.43	0.3099	0.64 ± 0.42	0.5992	0.76 ± 0.14	0.7847
SSA_{max} (cm^2)	0.001	24.4 ± 7.2	11.3 ± 4.1	0.0010	16.4 ± 3.0	0.0053	10.9 ± 1.9	0.0004	19.9 ± 2.0	0.1696

Values are mean ± SD. CMR: cardiac magnetic resonance; SSAV: sweep surface area velocity; SSA: sweep surface area; S_{SSAV}: peak systolic SSAV; E_{SSAV}: peak SSAV during early diastolic filling; A_{SSAV}: peak SSAV during atrial contraction; SSA_{max}: maximal SSA; HF: heart failure; rTOF: repaired tetralogy of Fallot; PH: pulmonary hypertension; HCM: hypertrophic cardiomyopathy.

[$] Adjusted for age.

96.2 $cm^2\ s^{-1}$, $p < 0.05$) and SSA_{max} (11.3 ± 4.1 vs. 24.4 ± 7.2 cm^2, $p < 0.05$) when compared to normal controls. Patients with PH had similar significant reduction in SSA and SSAV measurements with the single exception of A_{SSAV} which did not reach statistical significance (75.9 ± 17.3 vs. 157.3 ± 96.2 $cm^2\ s^{-1}$, $p = 0.061$). Patients in the rTOF group had significantly reduced S_{SSAV} (77.3 ± 21.4 vs. 129.7 ± 44.2 $cm^2\ s^{-1}$, $p < 0.05$), A_{SSAV} (71.1 ± 18.4 vs. 157.3 ± 96.2 $cm^2\ s^{-1}$, $p < 0.05$) and SSA_{max} (16.4 ± 3.0 vs. 24.4 ± 7.2 cm^2, $p < 0.05$) in comparison to the controls.

Reproducibility

Table 5 summarizes the results of intra- and inter-observer reproducibility analysis. The CMR derived measurements demonstrated excellent consistency as reflected by Pearson's correlation (ranges: intra-observer, 0.995–0.982; inter-observer, 0.997–0.975) and ICC (ranges: intra-observer, 0.995–0.977; inter-observer, 0.997–0.975) with no significant bias and narrow limits of agreement for both intra-observer and inter-observer measurements.

DISCUSSION

This study provides several novel findings. First, a new CMR-based systematic tool and methodology for 3D TA motion assessment with multiple CMR planes has been validated in 16 normal controls, 6 HF patients, 5 rTOF patients, 5 PH patients and 6 HCM patients. Second, results show that the CMR-derived TA motion parameters in 3D provide higher diagnostic accuracy compared to that achieved using single 2D CMR plane (e.g., four-chamber view). Third, significant correlation was found between TA motion related measurements and information provided by RHC in patients whose disease required invasive procedure. Fourth, two new CMR-based diagnostic markers SSA and SSAV are introduced and shown to be effective in further quantifying 3D changes of TA motion. Finally, the CMR-derived TA measurements were highly reproducible, thus allowing this technique to be used in clinical practice and research.

The importance of assessment of TA motion has been demonstrated in several studies.[1,11,34,39] One study[34] analyzed 44 patients with HF (class II-III) and 30 age- and gender-matched healthy volunteers using standard and pulsed Doppler tissue echocardiography and revealed significant correlation between peak systolic TA velocity and the RVEF assessed by first-pass radionuclide ventriculography ($r = 0.648$, $p < 0.001$). The value of peak systolic TA velocity < 11.5 cm s^{-1}

TABLE 5. Results of intra-observer and inter-observer reproducibility analysis, expressed as Pearson's correlation coefficient, Bland–Altman analysis and ICC.

	Intra-observer (2 controls, 2 HF, 2 rTOF)			Inter-observer (2 controls, 2 HF, 2 rTOF)		
	r	Bias	ICC (95% CI)	*r*	Bias	ICC (95% CI)
Sm	0.993	0.010 (−0.960 to 0.981)	0.992 (0.983–0.996)	0.997	−0.060 (−0.720 to 0.605)	0.997 (0.993– 0.999)
Em	0.995	−0.004 (−1.201 to 1.194)	0.995 (0.990–0.998)	0.993	−0.277 (−1.831 to 1.277)	0.992 (0.984–0.996)
Am	0.982	0.180 (−1.996 to 2.356)	0.977 (0.953–0.989)	0.986	−0.130 (−1.750 to 2.013)	0.984 (0.966–0.992)
Em/Am	0.989	−0.020 (−0.293 to 0.257)	0.988 (0.976–0.994)	0.975	−0.010 (−0.404 to 0.389)	0.975 (0.946–0.988)

ICC: Intra-class correlation coefficient; CI: confidence interval; Sm: peak TA systolic velocity; Em: peak TA velocity during early diastolic filling; Am: peak TA velocity during atrial contraction; HF: heart failure; rTOF: repaired tetralogy of Fallot.

predicted the presence of RV dysfunction (RVEF < 45%) with a sensitivity of 90% and a specificity of 85%.[34] Another study involving 71 consecutive patients with a first acute myocardial infarction (MI) has suggested that TA motion and velocity were significantly decreased and hence can be used to assess RV function in association with inferior MI.[1]

Technical Considerations of This Study

Modality Selection

The present study unveiled the relationship between CMR imaging and TA motion assessment. Currently, clinicians use M-mode echocardiography and tissue Doppler imaging (TDI) to measure regional TA velocity, displacement and timing at the RV free wall level. The angle dependency is a serious limitation for all Doppler-based techniques, however, including Doppler-derived myocardial velocities. It is also not unusual to have some variation in peak velocity amplitude and timing by subtle changes in the sample volume positioning.[25] The number of RV segments that can be assessed by TDI is limited, and only measurements of septum-to-RV free wall dyssynchrony are feasible.[49] Moreover, attainment of standard RV views may be difficult in practice because the RV free wall may not be optimally imaged from typical echocardiographic windows due to its anterior location and lung interference.[19] In contrast, the present study adopted CMR imaging to evaluate the 3D TA motion for RV systolic and diastolic function assessment. Compared to echocardiography, CMR has high spatial resolution, excellent tissue characterization, and free spatial orientation of imaging planes. The proposed CMR-based procedure is automated, reproducible, and efficient.

CMR Plane Selection

We hypothesized that comprehensive assessment of regional TA motion in 3D may provide novel insights into RV pathophysiologic mechanism and function. Hence, multiple CMR planes (four-chamber, RV three-chamber, RV two-chamber) were selected to cover the tricuspid annulus across its septal, anterior, free wall, and inferior components. The long-axis four-chamber view is a basic planar representation for studying the right ventricle and is routinely obtained in conventional cardiac MRI protocols. The right two- and three-chamber views are specific planes recommended when there is clinical suspicion of RV involvement.[7] Further insights into the 3D TA motion can be acquired from the in-depth analysis in terms of velocity distribution and time differences in peak systolic and diastolic velocities along the tricuspid annulus.

Tracking Method

Accurate and time efficient tracking of TA motion in selected CMR planes is crucial to the subsequent extraction of motion parameters. The general motion of TA points observed in each CMR plane involves three components: translation, rotation and deformation. In fact, the major component of TA motion can be described as translational motion with superimposed slow-varying rotational and deformational motion. Hence, a simple—yet effective and reliable—tracking method incorporating adaptive template matching was adopted in this study. The translational TA motion between consecutive frames was determined using basic template matching, and the tracking errors due to all the non-translational transformations were minimized by iterative updates of template throughout the cardiac cycle.

Sweep Surface Area Velocity

Two novel indices (SSA and SSAV) were proposed to further quantify and assess 3D TA motion. These indices measure the "swept area change" globally and regionally along the reconstructed tricuspid annulus. Several studies have addressed the assessment of TA geometry and anatomy using 2D echocardiography,[45] computed tomography,[47] and real-time 3D

echocardiography.[2] The present study has demonstrated a potential CMR-based methodology for evaluating not only the TA configuration but also its dynamic behaviour and trajectory during the cardiac cycle. By considering the 3D TA motion as a whole (in both radial and longitudinal directions), the proposed method and parameters provide good morphological visualization and functional description of the tricuspid annulus.

Clinical Aspects of This Study

Diagnostic Marker Set

The present study provides a novel CMR-based RV diagnostic solution and a set of markers comprising of the following:

- *Regional* and *global* peak systolic and diastolic velocities and ratio {Sm (S_{SSAV}), Em (E_{SSAV}), Am (A_{SSAV}), Em/Am (E_{SSAV}/A_{SSAV})}; and maximal displacement {TAPSE (SSA_{max})}.
- Time to regional peak velocities {T-Sm, T-Em, T-Am} and maximal displacements {T-TAPSE}; and standard deviation for these regional timing values {SD T-Sm, SD T-Em, SD T-Am, SD T-TAPSE}.

The former are related to the RV function in terms of ventricular pumping ability and cardiac output, and the latter quantify RV dyssynchrony.

CMR TA Motion Parameters Among Patient Groups

In the present study, we observed significant differences pertaining to the TA motion among the enrolled patient groups. First, the peak systolic (Sm) and diastolic (Em and Am) velocities, as well as maximal displacement (TAPSE), were significantly reduced in HF patients in comparison with normal controls. These outcomes were consistent with earlier studies[34] and support the hypothesis that the RV dysfunction may develop in association with LV dysfunction *via* multiple mechanisms as indicated in Voelkel *et al.*[48] Patients in the rTOF group had reduced (albeit not statistically significant) TA velocity Em during early diastolic filling and a significantly lower peak systolic velocity Sm, late diastolic TA velocity Am during atrial contraction, and TAPSE in systole as compared with normal controls. These findings were in line with prior studies that have consistently found systolic and diastolic abnormalities in patients with rTOF.[41,46] Significant decreases in both systolic (Sm) and diastolic velocities (Em, Am) were observed in patients with PH. In the presence of RV pressure overload, as occurs in PH patients, the RV function decline is related more to loss of RV transversal displacement than to longitudinal shortening.[27,33] The current CMR-based method is advantageous in this respect as it is an angle independent technique, thus avoiding the limitations of TDI related to translational cardiac motion. The diastolic function of the right ventricle in patients with HCM tended to be impaired, with reduced Em and Am velocities, which agreed with earlier work suggesting that ventricular interdependence and increased chamber stiffness may constitute the possible mechanisms of RV diastolic dysfunction.[16,43]

Second, patients with HF, rTOF and PH had greater intra-ventricular contractile timing dyssynchrony, which was quantified by differences in motion timing among 6 TA sites from 3 CMR views as compared with controls. Similar results have been presented in[5,24,30] demonstrating dyssynchronous TA motion in these patient groups. It is well established that cardiac resynchronization therapy (CRT) can improve cardiac function and enhance functional capacity in selected HF patients. Studies have indicated that the beneficial effects of CRT are related mainly to the reduction of mechanical dyssynchrony within the left and/or right ventricle with subsequent improvement in pumping efficiency.[3,29] Hence, assessment of ventricular mechanical dyssynchrony from 3D CMR may be useful for future guidance of CRT.

Systolic RV Function

The assessment of systolic RV dysfunction provides significant diagnostic, therapeutic, and prognostic information in patients with congenital and acquired heart disease such as rTOF and congestive HF.[13,38] RVEF is a widely adopted clinical parameter for systolic RV function assessment. The present study investigated TA motion parameters derived from CMR and observed good overall correlation between RVEF and the 6-point average Sm and TAPSE for all enrolled subjects. Moreover, results have demonstrated better diagnostic accuracy of Sm and TAPSE by CMR as compared to RVEF (Table 3).

Systolic HF (SHF) and diastolic HF (DHF) are the two clinical subsets of HF syndrome most frequently encountered in clinical practice. Although DHF has been increasingly recognized,[4,26,35,37,40] clinical diagnosis remains challenging due to lack of knowledge of the underlying mechanisms which produce myocardial structural and functional changes in this syndrome. RVEF is relatively non-informative in diagnosing DHF, since patients with DHF typically exhibit ventricular EF within the normal range. The present study suggests that TA peak systolic velocity Sm and maximal displacement TAPSE may be more sensitive for detecting systolic dysfunction than RVEF in the HF patient group.

Global RV volume and EF obtained from CMR are commonly used clinically in the management of rTOF patients. RVEF from CMR is a superposition of all contributions of RV inflow tract, apical trabecular, and RVOT. A prior study[10] investigating regional function showed that reduction of global RVEF in rTOF patients was attributable more to lower EF in the RV inflow and outflow regions, and less to lower EF in the trabecular region. These regional functional measurements provided new insights into RV remodelling in rTOF. Similarly, current CMR-based evaluation of TA motion in a regional context may also be informative in diagnosing deteriorated regional myocardial motion and abnormalities in the TA contractile pattern in rTOF group.

Relationship to Invasive Hemodynamic Measurements

Current study provided an informative evaluation showing how the TA motion related measurements compare with information provided by the gold standard method—RHC—in patients with PH who had indication for invasive procedure. We could not find any previous study correlating TA motion parameters with RHC derived RV dP/dt_{max} but Demirkol *et al.*[42] showed that the RV dP/dt obtained from Doppler echocardiography had good correlation with tricuspid Sm velocity and TAPSE in healthy subjects. Similar results were also reported in Demirkol *et al.*[14] showing significant correlation between echocardiography based RV dP/dt and RV systolic function classified on the basis of TAPSE and TDI Sm velocity in patients with mitral stenosis. Our results suggested that the systolic TA motion parameters derived by CMR imaging can be used as informative surrogate markers of RV function.

Potential Clinical Impact of SSAV

Our TA motion evaluation was further extended based on CMR-based SSAV and SSA, which reflect radial, longitudinal and circumferential changes of the tricuspid annulus. The much smaller peak SSAV values and maximal SSA (Table 4) implied a slow and irregular motion of tricuspid annulus in the HF and rTOF patient groups. Results in the present study suggest that SSA and SSAV of the 3D tricuspid annulus are novel and valuable clinical indicators for RV assessment in patients with diverse heart diseases. The 3D TA reconstruction and SSAV extraction are clinically useful in terms of (1) quantifying RV systolic and diastolic function, (2) assessing tricuspid valve function, (3) monitoring ventricular remodelling in patients after heart attack, (4) enhancing the indication of CRT, and (5) evaluating the effectiveness of medical/surgical therapy in patients.

STUDY LIMITATIONS

There were limitations in this study, including a small number of enrolled subjects. A significantly larger clinical study on the CMR-based TA motion assessment stratified by gender, age, and other patient characteristics in a larger cohort of patients remains a laudable future goal. The present study aimed to introduce a new CMR-based systematic tool for 3D TA motion assessment. A deeper and more complete understanding of TA morphology and dynamic behaviour in a large cohort of human subjects, using the proposed methodology, would contribute importantly to TA pathophysiological knowledge, with ensuing impact on clinical diagnosis and surgical treatment.

ACKNOWLEDGMENTS

This work was funded by Biomedical Research Council under Singapore-China Joint Research Programme (BMRC 14/1/32/24/0002 for LZ) and the Goh Cardiovascular Research Grant (Duke-NUS-GCR/2013/0009 for LZ). The authors appreciate the support and medical editing assistance from Duke-NUS/SingHealth Academic Medicine Research Institute.

CONFLICT OF INTEREST

The author(s) have no conflicts of interest, financial or otherwise.

REFERENCES

[1]Alam, M., J. Wardell, E. Andersson, B. A. Samad, and R. Nordlander. Right ventricular function in patients with first inferior myocardial infarction: assessment by tricuspid annular motion and tricuspid annular velocity. *Am. Heart J.* 139:710–715, 2000.

[2]Anwar, A. M., M. L. Geleijnse, O. I. Soliman, J. S. McGhie, R. Frowijn, A. Nemes, A. E. van den Bosch, T. W. Galema, and F. J. Ten Cate. Assessment of normal tricuspid valve anatomy in adults by real-time three-dimensional echocardiography. *Int. J. Cardiovasc. Imaging* 23:717–724, 2007.

[3]Bax, J. J., G. B. Bleeker, T. H. Marwick, S. G. Molhoek, E. Boersma, P. Steendijk, E. E. van der Wall, and M. J. Schalij. Left ventricular dyssynchrony predicts response and prognosis after cardiac resynchronization therapy. *J. Am. Coll. Cardiol.* 44:1834–1840, 2004.

[4]Bhatia, R. S., J. V. Tu, D. S. Lee, P. C. Austin, J. Fang, A. Haouzi, Y. Gong, and P. P. Liu. Outcome of heart failure with preserved ejection fraction in a population-based study. *N. Engl. J. Med.* 355:260–269, 2006.

[5]Bleeker, G. B., J. J. Bax, P. Steendijk, M. J. Schalij, and E. E. van der Wall. Left ventricular dyssynchrony in patients

with heart failure: pathophysiology, diagnosis and treatment. *Nat. Clin. Pract. Cardiovasc. Med.* 3:213–219, 2006.
[6]Bleeker, G. B., P. Steendijk, E. R. Holman, C. M. Yu, O. A. Breithardt, T. A. M. Kaandorp, M. J. Schalij, E. E. van der Wall, P. Nihoyannopoulos, and J. J. Bax. Assessing right ventricular function: the role of echocardiography and complementary technologies. *Heart* 92(Suppl 1):i19–i26, 2006.
[7]Capelastegui Alber, A., E. Astigarraga Aguirre, M. A. de Paz, J. A. Larena Iturbe, and T. Salinas Yeregui. Study of the right ventricle using magnetic resonance imaging. *Radiologia* 54:231–245, 2012.
[8]Cawley, P. J., J. H. Maki, and C. M. Otto. Cardiovascular magnetic resonance imaging for valvular heart disease: technique and validation. *Circulation* 119:468–478, 2009.
[9]Chen, S. S. M., J. Keegan, A. W. Dowsey, T. Ismail, R. Wage, W. Li, G. Z. Yang, D. N. Firmin, and P. J. Kilner. Cardiovascular magnetic resonance tagging of the right ventricular free wall for the assessment of long axis myocardial function in congenital heart disease. *J. Cardiovasc. Magn. Reson.* 13:80, 2011.
[10]Cossor, W. J., F. Maffessanti, K. Addetia, V. Mor-Avi, K. Kawaji, D. Roberson, K. Dill, R. Lang, and A. Patel. Regional right ventricular ejection fraction and cardiac output in repaired tetralogy of Fallot***. *J. Am. Coll. Cardiol.* 2015. doi:10.1016/S0735-1097(15)60565-4.
[11]D'Andrea, A., P. Caso, S. Severino, B. Sarubbi, A. Forni, G. Cice, N. Esposito, M. Scherillo, M. Cotrufo, and R. Calabrò. Different involvement of right ventricular myocardial function in either physiologic or pathologic left ventricular hypertrophy: a Doppler tissue study. *J. Am. Soc. Echocardiogr.* 16:154–161, 2003.
[12]De Berg, M., O. Cheong, M. van Kreveld, and M. Overmars. Computational Geometry: Algorithms and Applications. Berlin: Springer, 2008.
[13]De Groote, P., A. Millaire, C. Foucher-Hossein, O. Nugue, X. Marchandise, G. Ducloux, and J. M. Lablanche. Right ventricular ejection fraction is an independent predictor of survival in patients with moderate heart failure. *J. Am. Coll. Cardiol.* 32:948–954, 1998.
[14]Demirkol, S., M. Unlü, Z. Arslan, O. Baysan, S. Balta, I. H. Kurt, U. Küçük, and T. Celik. Assessment of right ventricular systolic function with dP/dt in healthy subjects: an observational study. *Anadolu. Kardiyol. Derg.* 13:103–107, 2013.
[15]Dorosz, J. L., D. C. Lezotte, D. A. Weitzenkamp, L. A. Allen, and E. E. Salcedo. Performance of 3-dimensional echocardiography in measuring left ventricular volumes and ejection fraction: a systematic review and meta-analysis. *J. Am. Coll. Cardiol.* 59:1799–1808, 2012.
[16]Efthimiadis, G. K., G. E. Parharidis, H. I. Karvounis, K. D. Gemitzis, I. H. Styliadis, and G. E. Louridas. Doppler echocardiographic evaluation of right ventricular diastolic function in hypertrophic cardiomyopathy. *Eur. J. Echocardiogr.* 3:143–148, 2002.
[17]Gondi, S., and H. Dokainish. Right ventricular tissue Doppler and strain imaging: ready for clinical use. *Echocardiography* 24:522–532, 2007.
[18]Gonzalez, R. C., and R. E. Woods. Digital Image Processing. Upper Saddle River, NJ: Prentice-Hall, 2006.
[19]Greyson, C. R. Evaluation of right ventricular function. *Curr. Cardiol. Rep.* 13:194–202, 2011.
[20]Guendouz, S., S. Rappeneau, J. Nahum, J. L. Dubois-Randé, P. Gueret, J. L. Monin, P. Lim, S. Adnot, L. Hittinger, and T. Damy. Prognostic significance and normal values of 2D strain to assess right ventricular systolic function in chronic heart failure. *Circ. J.* 76:127–136, 2012.
[21]Haddad, F., S. A. Hunt, D. N. Rosenthal, and D. J. Murphy. Right ventricular function in cardiovascular disease, part I: anatomy, physiology, aging, and functional assessment of the right ventricle. *Circulation* 117:1436–1448, 2008.
[22]Horton, K. D., R. W. Meece, and J. C. Hill. Assessment of the right ventricle by echocardiography: a primer for cardiac sonographers. *J. Am. Soc. Echocardiogr.* 22:776–792, 2009.
[23]Ito, S., D. B. McElhinney, R. Adams, P. Bhatla, S. Chung, and L. Axel. Preliminary assessment of tricuspid valve annular velocity parameters by cardiac magnetic resonance imaging in adults with a volume-overloaded right ventricle: comparison of unrepaired atrial septal defect and repaired tetralogy of Fallot. *Pediatr. Cardiol.* 36:1294–1300, 2015.
[24]Jing, L., C. M. Haggerty, J. D. Suever, S. Alhadad, A. Prakash, F. Cecchin, O. Skrinjar, T. Geva, A. J. Powell, and B. K. Fornwalt. Patients with repaired tetralogy of Fallot suffer from intra- and inter-ventricular cardiac dyssynchrony: a cardiac magnetic resonance study. *Eur. Heart J. Cardiovasc. Imaging* 15:1333–1343, 2014.
[25]Kadappu, K., and L. Thomas. Tissue Doppler imaging in echocardiography: value and limitations. *Heart Lung Circ.* 24:224–233, 2015.
[26]Kass, D. A., J. G. Bronzwaer, and W. J. Paulus. What mechanisms underlie diastolic dysfunction in heart failure? *Circ. Res.* 94:1533–1542, 2004.
[27]Kind, T., G. J. Mauritz, J. T. Marcus, M. van de Veerdonk, N. Westerhof, and A. Vonk-Noordegraaf. Right ventricular ejection fraction is better reflected by transverse rather than longitudinal wall motion in pulmonary hypertension. *J. Cardiovasc. Magn. Res.* 12:35, 2010.
[28]Kreyszig, E. Advanced Engineering Mathematics, 9th ed. New York: Wiley, 2005, 816 pp.
[29]Leclercq, C., and D. A. Kass. Retiming the failing heart: principles and current clinical status of cardiac resynchronization. *J. Am. Coll. Cardiol.* 39:194–201, 2002.
[30]López-Candales, A., K. Dohi, N. Rajagopalan, M. Suffoletto, S. Murali, J. Gorcsan, and K. Edelman. Right ventricular dyssynchrony in patients with pulmonary hypertension is associated with disease severity and functional class. *Cardiovasc. Ultrasound* 3:23, 2005.
[31]Marcos, P., W. G. Vick, D. J. Sahn, M. Jerosch-Harold, A. Shurman, and F. H. Sheehan. Correlation of right ventricular ejection fraction and tricuspid annular plane systolic excursion in tetralogy of Fallot by magnetic resonance imaging. *Int. J. Cardiovasc. Imaging* 25:263–270, 2009.
[32]Matthews, J. C., T. F. Dardas, M. P. Dorsch, and K. D. Aaronson. Right sided heart failure: diagnosis and treatment strategies. *Curr. Treat Options Cardiovasc. Med.* 10:329–341, 2008.
[33]Mauritz, G. J., T. Kind, J. T. Marcus, H. J. Bogaard, M. van de Veerdonk, P. E. Postmus, A. Boonstra, N. Westerhof, and A. Vonk-Noordegraaf. Progressive changes in right ventricular geometric shortening and long-term survival in pulmonary arterial hypertension. *Chest* 141:935–943, 2012.
[34]Meluzin, J., L. Spinarova, J. Bakala, J. Toman, J. Krejcí, P. Hude, T. Kára, and M. Soucek. Pulsed Doppler tissue imaging of the velocity of tricuspid annular systolic motion. *Eur. Heart J.* 22:340–348, 2001.
[35]Moller, J. E., P. A. Pellikka, G. S. Hillis, and J. K. Oh. Prognostic importance of diastolic function and filling

pressure in patients with acute myocardial infarction. *Circulation* 114:438–444, 2006.
[36]Nijveldt, R., T. Germans, G. P. McCann, A. M. Beek, and A. C. van Rossum. Semi-quantitative assessment of right ventricular function in comparison to a 3D volumetric approach: a cardiovascular magnetic resonance study. *Eur. Radiol*. 18:2399–2405, 2008.
[37]Owan, T. E., D. O. Hodge, R. M. Herges, S. J. Jacobsen, V. L. Roger, and M. M. Redfield. Trends in prevalence and outcome of heart failure with preserved ejection fraction. *N. Engl. J. Med*. 355:251–259, 2006.
[38]Piran, S., G. Veldtman, S. Siu, G. D. Webb, and P. P. Liu. Heart failure and ventricular dysfunction in patients with single or systemic right ventricles. *Circulation* 105:1189–1194, 2002.
[39]Rajagopalan, N., K. Dohi, M. A. Simon, M. Suffoletto, K. Edelman, S. Murali, and A. López-Candales. Right ventricular dyssynchrony in heart failure: a tissue Doppler imaging study. *J. Card. Fail*. 12:263–267, 2006.
[40]Redfield, M. M., S. J. Jacobsen, J. C. Burnett, Jr, D. W. Mahoney, K. R. Bailey, and R. J. Rodeheffer. Burden of systolic and diastolic ventricular dysfunction in the community: appreciating the scope of the heart failure epidemic. *JAMA* 289:194–202, 2003.
[41]Riesenkampff, E., L. Mengelkamp, M. Mueller, S. Kropf, H. Abdul-Khaliq, S. Sarikouch, P. Beerbaum, R. Hetzer, P. Steendijk, F. Berger, and T. Kuehne. Integrated analysis of atrioventricular interactions in tetralogy of Fallot. *Am. J. Physiol. Heart Circ. Physiol*. 299:H364–H371, 2010.
[42]Sadeghpour, A., H. Harati, M. Kiavar, M. Esmaeizadeh, M. Maleki, F. Noohi, Z. Ojaghi, N. Samiea, A. Mohebbi, and H. Bakhshandeh. Correlation of right ventricular dp/dt with functional capacity and RV function in patients with mitral stenosis. *Int. Cardiovasc. Res. J*. 1:208–215, 2008.
[43]Santamore, W. P., and L. J. Dell'Italia. Ventricular interdependence: significant left ventricular contributions to right ventricular systolic function. *Prog. Cardiovasc. Dis*. 40:289–308, 1998.
[44]Szmigielski, C., K. Rajpoot, V. Grau, S. G. Myerson, C. Holloway, J. A. Noble, R. Kerber, and H. Becher. Real-time 3D fusion echocardiography. *JACC Cardiovasc. Imaging* 3:682–690, 2010.
[45]Tei, C., J. P. Pilgrim, P. M. Shah, J. A. Ormiston, and M. Wong. The tricuspid valve annulus: study of size and motion in normal subjects and in patients with tricuspid regurgitation. *Circulation* 66:665–671, 1982.
[46]van der Hulst, A. E., J. J. Westenberg, V. Delgado, L. J. Kroft, E. R. Holman, N. A. Blom, J. J. Bax, A. de Roos, and A. A. Roest. Tissue-velocity magnetic resonance imaging and tissue Doppler imaging to assess regional myocardial diastolic velocities at the right ventricle in corrected pediatric tetralogy of Fallot patients. *Invest. Radiol*. 47:189–196, 2012.
[47]van Rosendael, P. J., E. Joyce, S. Katsanos, P. Debonnaire, V. Kamperidis, F. van der Kley, M. J. Schalij, J. J. Bax, N. Ajmone Marsan, and V. Delgado. Tricuspid valve remodelling in functional tricuspid regurgitation: multidetector row computed tomography insights. *Eur. Heart J. Cardiovasc. Imaging* 17:96–105, 2016.
[48]Voelkel, N. F., R. A. Quaife, L. A. Leinwand, R. J. Barst, M. D. McGoon, D. R. Meldrum, J. Dupuis, C. S. Long, L. J. Rubin, F. W. Smart, Y. J. Suzuki, M. Gladwin, E. M. Denholm, and D. B. Gail. Right ventricular function and failure: report of a National Heart, Lung, and Blood Institute working group on cellular and molecular mechanisms of right heart failure. *Circulation* 114:1883–1891, 2006.
[49]Yu, C. M., E. Chau, J. E. Sanderson, K. Fan, M. O. Tang, W. H. Fung, H. Lin, S. L. Kong, Y. M. Lam, M. R. S. Hill, and C. P. Lau. Tissue Doppler echocardiographic evidence of reverse remodeling and improved synchronicity by simultaneously delaying regional contraction after biventricular pacing therapy in heart failure. *Circulation* 105:438–445, 2002.
[50]Zhong, L., L. Gobeawan, Y. Su, J. L. Tan, D. Ghista, T. Chua, R. S. Tan, and G. Kassab. Right ventricular regional wall curvedness and area strain in patients with repaired tetralogy of Fallot. *Am. J. Physiol. Heart Circ. Physiol*. 302:H1306–H1316, 2012.